

Interdigitated ring electrodes: Theory and experiment

Edward O. Barnes^a, Ana Fernández la Villa^b, Diego F. Pozo Ayuso^b,
Mario Castaño Alvarez^b, Grace E. M. Lewis^c, Sara E. C. Dale^c,
Frank Marken^c and Richard G. Compton^{a*}

*Corresponding author

Email: richard.compton@chem.ox.ac.uk

Fax: +44 (0) 1865 275410; Tel: +44 (0) 1865 275413.

^aDepartment of Chemistry, Physical and Theoretical Chemistry Laboratory,
Oxford University, South Parks Road, Oxford, OX1 3QZ, United Kingdom.

^bMicruX Fluidic, S.L., Edificio Severo Ochoa, Julián Clavería, s/n, 33006 Oviedo (Asturias),
Spain.

^cDepartment of Chemistry, University of Bath, Bath, BA2 7AY, United Kingdom.

To be submitted as an article to:

The Journal of Electroanalytical Chemistry

Abstract

The oxidation of potassium ferrocyanide, $\text{K}_4\text{Fe}(\text{CN})_6$, in aqueous solution under fully supported conditions is carried out at interdigitated band and ring electrode arrays, and compared to theoretical models developed to simulate the processes. Simulated data is found to fit well with experimental results using literature values of diffusion coefficients for $\text{Fe}(\text{CN})_6^{4-}$ and $\text{Fe}(\text{CN})_6^{3-}$. The theoretical models are used to compare responses from interdigitated band and ring arrays, and the size of ring array required to approximate the response to a linear band array is investigated. An equation is developed for the radius of ring required for a pair of electrodes in a ring array to give a result with 5% of a pair of electrodes in a band array. This equation is found to be independent of the scan rate used over six orders of magnitude.

Keywords

electrochemical simulation, electrode arrays, generator-collector systems, interdigitated band electrodes, interdigitated ring electrodes

1 Introduction

Microelectrode arrays are increasingly employed in electrochemistry,^{1,2} since they can provide the advantages of microelectrodes (fast mass transport, the use of two rather than three electrode control, observation of steady state currents) whilst providing the large currents usually associated with macroelectrodes. These arrays also have considerably less capacitive current than macroelectrodes, although generally more than isolated microelectrodes, representing an intermediate case.³ However, while single microelectrodes typically have a much smaller ohmic drop than macroelectrodes (due to the smaller currents drawn), a microelectrode array has significantly larger ohmic drop than a macroelectrode of equivalent overall area.¹ The main types of array electrodes are arrays of microdiscs (where the array may be regular or random) and arrays of microbands.

Microband arrays, as well as a single pair of bands, have been used as generator-collector systems,⁴⁻¹² with great success. In a collector generator system, some target species in solution is oxidised (or reduced) at the generator electrode, with the product of this reaction then detected by re-reduction (or oxidation) at the collector electrode. If single step chronoamperometry, for example, were to be carried out, then some species might be oxidised at the generator electrode to produce species B, which would then be reduced at the collector electrode, both under diffusion control:



An important feature in an experiment of this type is the collection efficiency, N , the ratio of the collector current to the generator current:

$$N = -\frac{I_{\text{col}}}{I_{\text{gen}}} \quad (3)$$

This simple experiment can be extended to performing cyclic voltammetry at the generator electrode, while keeping the collector electrode fixed at the potential to reduce species B. This approach has been used to study, for example, competing modes of transport at a phase boundary (transport along the interface vs transport in bulk).¹³ Other uses of collector generator systems include mechanistic investigations,^{14–17} probing intermediate kinetics,^{18,19} electrochemical sensing with very low detection limits,²⁰ targeted detection of one species in the presence of another,²¹ and the simultaneous measurement of two species.²²

Microband arrays lend themselves particularly well to generator-collector systems. They consist of a series of parallel bands, which alternate between being generator and collector. This is shown in Fig. 1a, and the apparatus is known as an interdigitated array (IDBA). This ensures a very high collection efficiency,²³ since any species produced at the generator electrode is likely to diffuse to the collector electrode with a high probability of detection if the separation is small. This spatial arrangement also allows for efficient redox cycling,²³ where species cycle between generator and collector electrodes, enhancing the measured current.

IDBAs have been used to simultaneously measure both the concentration and diffusion coefficient of a species. Aoki *et. al.*⁸ developed a theoretical equation for the steady state current produced at a parallel microband array electrode during a chronoamperometric experiment as

outlined above:

$$I_{SS} = nFDc^*l \frac{K(1-p)}{K(p)} \quad (4)$$

where I_{ss} is the steady state current (A), n is the number of electrons transferred, F is the Faraday constant, D is the diffusion coefficient of the species under investigation ($\text{m}^2 \text{s}^{-1}$), c^* is this species' bulk concentration (mol m^{-3}), l is the length of the individual band electrodes (m), and p is some function of the electrode geometry. The function K is a total elliptic integral, and $K(1-p)/K(p)$ can be approximated as:

$$\frac{K(1-p)}{K(p)} \approx 0.318 \ln \left[2.55 \left(1 + \frac{w_e}{w_g} \right) \right] - 0.095 \left(1 + \frac{w_e}{w_g} \right)^{-2} \quad (5)$$

where w_g and w_e are the inter-electrode distance and the electrode width respectively. Also developed was an empirical equation to describe the time taken for the current at the collector electrode to reach half of its steady state value, $t_{0.5}$:

$$t_{0.5} \approx 0.90 \frac{\left(w_g + \frac{w_e}{6} \right)^2}{D} \quad (6)$$

So by measuring the steady state current and the time taken for to reach half this value, equations 4 and 6 can be solved simultaneously to determine c^* and D .

A convenient and important variation on IDBAs are interdigitated ring electrode arrays, IDRA_s.²⁴ a schematic of an IDRA is shown in Fig. 1b. They consist of a central disc electrode (throughout this paper considered to be a generator electrode) surrounded by expanding concentric ring electrodes which alternate between collector and generator in character. The obvious difference between this and an IDBA is the cylindrical nature of the diffusion. The

radial component will, at least for rings of small radii, enhance the mass transport between the electrodes, leading to an increased rate of redox cycling and a greater current enhancement in comparison with linear IDBAs. For very large rings, however, the diffusion will become less cylindrical and these effects will be lost, with the behavior tending to that of parallel bands. This study investigates the extent to which this is the case, and explores how well experiments carried out at an IDRA can be simulated a simplified IDBA model.

2 Theory

Cyclic voltammetry is simulated at both linear interdigitated arrays (IDBAs) and interdigitated ring arrays (IDRAs), shown in Fig 1a and 1b respectively. In each case, a single electroactive species, A, is considered to be initially present in solution, along with a large amount of an inert electrolyte to suppress electric fields and render the mass transport diffusion only. The generator electrodes are subject to a linearly sweeping potential to set up a potential dependent equilibrium between species A and its oxidised form, species B, while the collector electrodes are set at a fixed potential to reduce species B at a mass transport controlled rate:



2.1 Interdigitated arrays

To simulate a linear interdigitated array, we make the assumption that the electrodes are much longer than they are wide, reducing the problem from three dimensions to two. The mass

transport equation is therefore:

$$\frac{\partial c_i}{\partial t} = D_i \left(\frac{\partial^2 c_i}{\partial x^2} + \frac{\partial^2 c_i}{\partial y^2} \right) \quad (9)$$

where c_i is the concentration of species i (mol m^{-3}) and D_i is the diffusion coefficient of species i ($\text{m}^2 \text{s}^{-1}$). All symbols are defined in Table 1. The simulation space which this is solved over is shown schematically in Fig. 2a. The mass transport equation is solved subject to boundary conditions. At the generator electrode surface, Butler-Volmer kinetics are applied:

$$D_A \left(\frac{\partial c_A}{\partial y} \right) = k^0 \left[c_A^0 \exp \left(\frac{-\alpha (E - E_f^\ominus)}{RT} \right) - c_B^0 \exp \left(\frac{(1 - \alpha) (E - E_f^\ominus)}{RT} \right) \right] \quad (10)$$

and equal fluxes of species are maintained by virtue of conservation of mass:

$$D_B \left(\frac{\partial c_B}{\partial y} \right) = -D_A \left(\frac{\partial c_A}{\partial y} \right) \quad (11)$$

At the collector electrode surface, the potential is such that species B is reduced to species A and a mass transport controlled rate, and equal fluxes are again maintained:

$$c_B = 0 \quad (12)$$

$$D_A \left(\frac{\partial c_A}{\partial y} \right) = -D_B \left(\frac{\partial c_B}{\partial y} \right) \quad (13)$$

The edges of the simulation space are set at the centres of the electrodes ($x_{\min} = -\frac{1}{2}w_g - w_e$ and $x_{\max} = \frac{1}{2}w_g + w_e$) a distance along the y axis from the electrodes known to be well outside the diffusion layer^{25,26} ($y_{\max} = 6\sqrt{D_{\max}t_{\max}}$) where D_{\max} and t_{\max} are the largest diffusion

coefficient in the system, and the total time of the experiment. At the simulation edges, a zero flux condition is imposed on all species:

$$\left(\frac{\partial c_i}{\partial x}\right)_{x_{\min}, x_{\max}, \text{all } y} = 0 \quad (14)$$

$$\left(\frac{\partial c_i}{\partial y}\right)_{\text{all } x, y_{\max}} = 0 \quad (15)$$

$$(16)$$

The value of the potential applied to the generator electrode at a given time from the start of the experiment must also be defined. If the scan starts at some potential value E_s (V), and sweeps at a scan rate of ν (V s^{-1}) up to a vertex potential E_v (V) before reversing and scanning back to E_s , the the applied potential E at any given time t is:

$$E = E_v \pm |E_v - E_s \pm \nu t| \quad (17)$$

where $+$ is used for a reduction and $-$ for an oxidation.

2.1.1 Normalised Model

The above model is next simplified by introducing normalised (or “dimensionless”) variables to make it general. The bulk concentration of species A, for example, is merely a scaling factor and is set to 1, with all other concentrations calculated relative to this. Similarly, all diffusion coefficients are set relative to D_A , and all distances relative to the width of the electrode. A full list of normalised parameters and their definition is given in Table 2. The normalised simulation space is shown schematically in Fig. 2b. Upon the substitution of dimensional parameters for

normalised ones, the mass transport equation becomes:

$$\frac{\partial C_i}{\partial \tau} = D'_i \left(\frac{\partial^2 C_i}{\partial X^2} + \frac{\partial^2 C_i}{\partial Y^2} \right) \quad (18)$$

The normalised boundary conditions are summarised in Table 3. The normalised potential applied to the generator (θ) electrode is still a function of normalised scan rate, σ :

$$\theta = \theta_v \pm |\theta_v - \theta_s \pm \sigma \tau| \quad (19)$$

again with + used for a reduction and – for an oxidation.

2.1.2 Calculating the current at an IDBA

Upon the implementation of the above model, the current at both the generator and the collector electrodes must be calculated. The (dimensionless) flux density at an individual generator electrode is given by integrating the flux across its width:

$$j_{\text{gen}} = 2 \int_{-0.5-\frac{1}{2}d}^{-\frac{1}{2}d} D'_A \left(\frac{\partial C_A}{\partial Y} \right)_{Y=0} dX \quad (20)$$

and at the collector:

$$j_{\text{col}} = 2 \int_{\frac{1}{2}d}^{0.5+\frac{1}{2}d} D'_A \left(\frac{\partial C_A}{\partial Y} \right)_{Y=0} dX \quad (21)$$

Note the factors of 2, these are due to using the symmetry of an interdigitated array to simulate only half of an individual generator and collector electrode. The dimensional current is then

given by:

$$I = nFImDc_A^*j \quad (22)$$

where m is the number of generator-collector pairs.

2.2 Interdigitated ring arrays

To simulate an IDRA, the model developed above must be modified to account for the added radial nature of the diffusion. The new (dimensionless) mass transport equation is:

$$\frac{\partial C_i}{\partial \tau} = D_i' \left(\frac{\partial^2 C_i}{\partial R^2} + \frac{1}{R} \frac{\partial C_i}{\partial R} + \frac{\partial^2 C_i}{\partial Z^2} \right) \quad (23)$$

where R is the dimensionless radial coordinate and Z is the dimensionless coordinate perpendicular to the surface of the electrodes, as defined in Table 2. Fig. 3a and 3b show schematically the dimensional and normalised simulation space this equation is to be solved over. The key difference between this simulation space and that used for the IDBA model (Fig. 2) is that the whole width of the generator electrode is now included in the centre, with half of the two collector electrodes on either side. The central of the simulation space is now no longer zero, but set at a value R_0 , determined by the geometry of the IDRA being simulated. Some of the symmetry that was present in the IDBA model is lost due to the radial diffusion, which will be different on different sides of the generator electrode (due to the different values of R). The edge of the simulation space is in the centre of the collector electrodes, but unlike above where this was a result of symmetry, it is now an approximation.

The boundary conditions are analogous to those used in the IDBA model, and are given in

Table 4. The potential applied to the generator electrode, θ , varies with time and scan rate in exactly the same way as above.

2.2.1 Calculating the current at an IDRA

When calculating the current at an IDRA, it must be noted that since we are working in cylindrical coordinates, a factor of R must be included in the integrals to calculate the overall flux. So the flux at the generator electrode is given by:

$$j_{\text{gen}} = \int_{R_0-0.5}^{R_0+0.5} D'_A \left(\frac{\partial C_A}{\partial Z} \right)_{Z=0} \frac{R}{R_0} dR \quad (24)$$

and at the collector:

$$j_{\text{gen}} = \int_{R_0-d-1}^{R_0-d-0.5} D'_A \left(\frac{\partial C_A}{\partial Z} \right)_{Z=0} \frac{R}{R_0} dR + \int_{R_0+d+0.5}^{R_0+d+1} D'_A \left(\frac{\partial C_A}{\partial Z} \right)_{Z=0} \frac{R}{R_0} dR \quad (25)$$

(the factor $\frac{1}{R_0}$ is included to normalise the response with respect to R_0 and make for easier comparison of IBDA and IDRA responses.) The dimensional current can then be obtained from the expression:

$$I = 2\pi n F w_e R_0 D c_A^* j \quad (26)$$

$$= 2\pi n F r_0 D c_A^* j \quad (27)$$

This will give the current measured at one pair of generator-collector electrodes, at radial coordinate r_0 . To simulate the current measured at the entire array, many simulations must be run, each with a different value of r_0 , and the results summed together.

2.3 Numerical methods

The method of Crank and Nicolson²⁷ was used to discretise the mass transport equations and boundary conditions to allow them to be solved numerically. The alternating direction implicit method²⁸ was used, in conjunction with the Thomas algorithm²⁹ to efficiently solve the diagonal matrices produced.

The spatial grid the equations were solved over has been successfully employed previously to simulate an individual pair of parallel generator-collector microbands,³⁰ as well as at arrays of discs³¹ and hemispheres³². In the Y direction (for an IDBA, Z for an IDRA), the first grid point is at the electrode/insulating surface, and has an initial step size of Δ . The grid then expands away from this surface in the following manner:

$$Y_j = \gamma Y_{j-1} \quad (28)$$

The X (for an IDBA, R for an IDRA) grid is analogous to this, with the grid expanding away from the edges of the electrodes until it meets a grid coming in the other direction (into the centre of gaps or electrodes) or until it meets the edge of the simulation space.

The temporal grid is a regular array of points. For each unit of dimensionless potential, θ , the grid is defined to have N_θ points.

Convergence studies found the following grid parameters sufficient to produce results within 1% of a fully converged value: $\Delta = 8 \times 10^{-5}$, $\gamma = 1.125$, $N_\theta = 1 \times 10^4$. Simulations were run on an Intel (R) Xeon (R) 2.26 GHz PC with 2.25 GB RAM, with a typical running time of 20 mins per simulation.

3 Theoretical Results

In order to compare and contrast cyclic voltammetry at IDBAs and IDRAs, simulations were carried out at both geometries. A simple, fully electrochemically reversible one electron oxidation was simulated at a generator-collector pair within an IDBA and compared to the same reaction simulated at a generator-collector pair in an IDRA with various values of R_0 . The results for σ values of 0.001 (microelectrode/slow scan rate), 1 (intermediate) and 1000 (macroelectrode/fast scan rate) are shown in Fig. 4. In all cases, d' is fixed at 0.1, $D'_B = 1$, $\alpha = 0.5$ and $K^0 = 1000$. It is seen that for all scan rates, a smaller value of R_0 enhances the dimensionless current, due to the greater radial diffusion and more efficient mass transport. As R_0 tends to infinity, the IDRA responses converge onto the response obtained at an IDBA, since the electrodes become effectively linear. As expected, the collector electrode response becomes very small at large values of sigma, since in this limit the diffusion is largely planar, so species B does not diffuse outwards towards the collector electrode.

It will be useful to know how much the current at a pair of electrodes in an IDRA deviates from that measured at an IDBA as a function of R_0 . This deviation, or current enhancement, is defined here as Q , the ratio of the peak (or steady state) generator current simulated in a IDRA simulation to that simulated at an IDBA electrode with equal d' . From Fig. 4 it is seen that as R_0 decreases, the current enhancement ratio Q increases. Fig 5 shows the simulated values of Q for three values of d' (0.1, 0.5 and 0.9), each for the values of sigma (0.001, 1 and 1000). All other values remain the same as in Fig 4. It is seen that at small R_0 , Q rapidly drops off as R_0 increases, and approaches 1 as $R_0 \rightarrow \infty$. It is also seen that, for a given value of d' , the variation of Q with R_0 is essentially independent of σ over six orders of magnitude

(differences between Q values for any given R_0 is less than 1%).

Using these curves, it is then possible to calculate a value of R_0 at which Q is a specific value, for example 1.05. Any value of R_0 larger than this will then produce results at an IDRA within 5% of the result for an equivalent IDBA. This value of R_0 is labeled $R_{5\%}$. The value of $R_{5\%}$ for a given d' is calculated by performing six IDRA simulations with various R_0 which give values of Q between 1.04 and 1.06, and fitting a polynomial equation to the Q vs R_0 curve using the Microsoft Excel graph fitting tool (a cubic equation was found to be sufficient, higher orders produced no more accurate results). This equation can then be set equal to 1.05 and solved to give a value of $R_{5\%}$. This was done for values of d' between 0.1 and 1.0. For each d' , a range of scan rates between 0.001 and 1000 were used, and an average $R_{5\%}$ taken. The results are shown in Fig. 6. It is seen that, for this range of d' values, $R_{5\%}$ varies linearly with d' . A line of best fit was found using Microsoft Excel to be $R_{5\%} = 22.4d' + 19.7$.

In an IDRA, the overall measured current will be dominated by the outermost electrodes, since these are largest in area. Any pair of electrodes with an R coordinate at the centre of the generator greater than $R_{5\%}$ will produce currents within 5% of those produced at an IDBA. Hence, an IDRA whose outermost electrode pair satisfies this condition is likely to be able to be simulated with reasonable accuracy as an IDBA (weighting each electrode pair's contribution according to its size).

4 Experimental Methods

Potassium ferrocyanide ($K_4Fe(CN)_6$), potassium chloride (KCl) and nitrogen gas (N_2) were purchased from Sigma Aldrich (USA) and used as received, without purification. Solutions were

prepared in deionised water of resistivity of no less than 18.2 M Ω cm (Millipore). Solutions were thoroughly degassed by bubbling nitrogen (oxygen free) for at least 30 mins. Electrochemical experiments were carried out in a thermostated Faraday cage at 298 (\pm 1) K, using a PalmSens Bipotentiostat, (Palm Instruments BV, Netherlands). The platinum interdigitated ring/band working electrodes were fabricated by Micrux Technologies (Spain) using photolithographic techniques on a pyrex substrate. Platinum reference and counter electrodes are integrated by photolithography onto this substrate.

5 Experimental Results

5.1 Interdigitated band array

Cyclic voltammetry was carried out on aqueous 1 mM potassium ferrocyanide, $\text{K}_4\text{Fe}(\text{CN})_6$, at a scan rate of 50 mV s $^{-1}$ in the presence of 0.1 M KCl at three different Pt IDBA electrodes of varying geometries (summarised in Table 5). In all three cases the lengths of the electrodes is 2 mm. The results for IDBA1, IDBA2 and IDBA3 are shown in Fig. 7, along with theoretical best fits. Literature values for the diffusion coefficients^{33,34} of $\text{Fe}(\text{CN})_6^{4-}$ and $\text{Fe}(\text{CN})_6^{3-}$ of 6.6×10^{-12} m 2 s $^{-1}$ and 7.5×10^{-12} m 2 s $^{-1}$ respectively were used in the simulations, with a best fit concentration determined to be 0.95 ± 0.05 mM. α and β are set at 0.5, and k^0 is arbitrarily set at 1000 m s $^{-1}$ to ensure complete electrochemical reversibility. Excellent fits are seen, validating the IDBA model developed above. Collection efficiencies for IDBA1, 2 and 3 at the vertex potential were measured as 79%, 96% and 96%. This is consistent with smaller inter electrode gaps (relative to the electrode widths) producing higher collection efficiencies.

5.2 Interdigitated ring array

The cyclic voltammetry of aqueous 1 mM $\text{K}_4\text{Fe}(\text{CN})_6$ was then repeated on two Pt IDRA electrodes (geometries summarised in Table 5), again at a scan rate of 50 mV s^{-1} , in the presence of 0.1 M KCl. The experiments were simulated using the full IDRA model outlined above, and using the IDBA model with each pair of generator-collector electrodes having an area equal to each of the generator electrodes in the IDRAs. The results are shown in Fig. 8. Collection efficiencies at the potential vertex were measured as 78% and 92% for IDRA1 and 2 respectively, again reflective of the smaller gap size in IDRA2. For the simulations, the same literature diffusion coefficients as above were used, and in both cases the concentration of $\text{K}_4\text{Fe}(\text{CN})_6$ was fixed at 1 mM. It is seen that the two models produce very similar results, which both fit well with the experimental data, with differences likely being due to capacitive effects. The experimentally measured currents are dominated by the larger, more peripheral rings, which have small enough curvature for radial diffusion to be negligible on these timescales. For IDRA1, the outermost electrode pair has an R_0 value of 46. The equation for $R_{5\%}$ developed above gives an $R_{5\%}$ value of 42.16 for $d' = 1.0$, meaning this outer electrode pair can be reasonably well modelled as bands. For IDRA2, the outer electrode pair has $R_0 = 94.3$, well above the $R_{5\%}$ value of 33.18 for this geometry. This allows us to model these IDRAs using the computationally more simplistic IDBA model.

6 Conclusions

In this study, interdigitated band and ring electrodes were simulated and theoretical results compared. It was found that if a generator-collector pair of electrodes in a ring array has

a large enough radius, the pair can be approximated as a pair of parallel linear bands. An equation has been developed for what radius this pair in a ring array needs to be to produce a result within 5% of that at parallel bands: $R_0 \geq 22.4d' + 19.7$ in the range $0.1 \leq d' \leq 1.0$. This was found to be independent of the scan rate used. The models for interdigitated bands and rings were used to simulate experimental data for the oxidation of $\text{Fe}(\text{CN})_6^{4-}$, and found to give good fits. It was also shown that if the inequality given above is satisfied for the outermost pair of electrodes in a ring array, then the array can be effectively modelled using the more simplistic interdigitated band array model.

Acknowledgments

We thank EPSRC for financial support. EOB and GEML further than St John's College, Oxford and NERC for additional support.

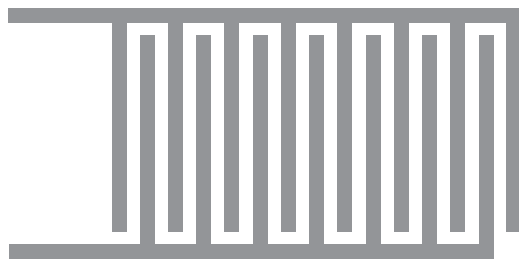
References

- [1] Ordeig, O.; del Campo, J.; Xavier Muñoz, F.; Banks, C. E.; Compton, R. G. *Electroanalysis* **2007**, *19*, 1973–1986.
- [2] Herzog, G.; Beni, V. *Anal. Chim. Acta* **2013**, *769*, 10 – 21.
- [3] Fletcher, S.; Horne, M. D. *Electrochem. Commun.* **1999**, *1*, 502–512.
- [4] Tomčík, P.; Jursa, S.; Mesároš, v.; Bustin, D. *J. Electroanal. Chem.* **1997**, *423*, 115–118.
- [5] Sanderson, D. G.; Anderson, L. B. *Anal. Chem.* **1985**, *57*, 2388–2393.
- [6] Jenčušová, P.; Tomčík, P.; Bustin, D.; Rievaj, M.; Dovalovská, Z. *Chem. Pap.* **2006**, *60*, 173–178.
- [7] Aoki, K.; Morita, M.; Niwa, O.; Tabei, H. *J. Electroanal. Chem.* **1988**, *256*, 269 – 282.
- [8] Aoki, K.; Tanaka, M. *J. Electroanal. Chem.* **1989**, *266*, 11 – 20.
- [9] Strutwolf, J.; Williams, D. E. *Electroanalysis* **2005**, *17*, 169–177.
- [10] Barnes, E. O.; Lewis, G. E. M.; Dale, S. E. C.; Marken, F.; Compton, R. G. *Analyst* **2012**, *137*, 1068–1081.
- [11] Rajantie, H.; Strutwolf, J.; Williams, D. E. *J. Electroanal. Chem.* **2001**, *500*, 108–120.
- [12] Rajantie, H.; Williams, D. E. *Analyst* **2001**, *126*, 1882–1887.
- [13] French, R. W.; Chan, Y.; Bulman-Page, P. C.; Marken, F. *Electrophoresis* **2009**, *30*, 3361–3365.

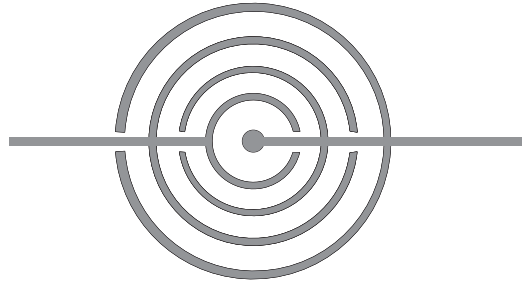
- [14] Nekrasov, L. N.; Khrushcheva, E. I. *Elektrokhimiya* **1967**, *3*, 166–172.
- [15] Damjanovic, A.; Genshaw, A. M. A.; Bockris, J. O. *J. Electrochem. Soc.* **1967**, *114*, 1107–1112.
- [16] Unwin, P. R. *J. Electroanal. Chem.* **1991**, *297*, 103 – 124.
- [17] Bruckenstein, S.; Miller, B. *Acc. Chem. Res.* **1977**, *10*, 54–61.
- [18] Albery, W. J.; Bruckenstein, S. *Trans. Faraday Soc.* **1966**, *62*, 1946–1954.
- [19] Albery, W. J.; Bruckenstein, S. *Trans. Faraday Soc.* **1966**, *62*, 2584–2595.
- [20] Dale, S. E. C.; Vuorema, A.; Ashmore, E. M. Y.; Kasprzyk-Hordén, B.; Sillanpää, M.; Denuault, G.; Marken, F. *Chem. Rec.* **2012**, *12*, 143–148.
- [21] Zhu, F.; Yan, J.; Lu, M.; Zhou, Y.; Yang, Y.; Mao, B. *Electrochim. Acta* **2011**, *56*, 8101 – 8107.
- [22] Barnes, E. O.; Lewis, G. E. M.; Dale, S. E. C.; Marken, F.; Compton, R. G. *J. Electroan* **2013**,
- [23] Niwa, O.; Morita, M.; Tabei, H. *Anal. Chem.* **1990**, *62*, 447–452.
- [24] Niwa, O.; Morita, M. *Anal. Chem.* **1996**, *68*, 355–359.
- [25] Gavaghan, D. J. *J. Electroanal. Chem.* **1998**, *456*, 1–12.
- [26] Svir, I. B.; Oleinick, A. I.; Compton, R. G. *Radiotekhnika* **2001**, *116*, 114.
- [27] Crank, J.; Nicolson, E. *Proc. Camb. Phil. Soc.* **1947**, *43*, 50–67.

- [28] Press, W. H., Teukolsky, S. A., Vetterling, W. T., Flannery, B. P., Eds. *Numerical Recipes: The Art of Scientific Computing*; Cambridge University Press, 2007.
- [29] Compton, R. G.; Pilkington, M. B. G.; Stearn, G. M. *J. Chem. Soc., Faraday Trans. 1* **1988**, *84*, 2155–2171.
- [30] Barnes, E.; Lewis, G.; Dale, S.; Marken, F.; Compton, R. *J. Electroanal. Chem.* **2013**, *703*, 38–44.
- [31] Ordeig, O.; Banks, C. E.; Davies, T. J.; del Campo, J.; Mas, R.; Muñoz, F. X.; Compton, R. G. *Analyst* **2006**, *131*, 440–445.
- [32] Ward, K. R.; Lawrence, N. S.; Hartshorne, R. S.; Compton, R. G. *J. Phys. Chem. C* **2011**, *115*, 11204–11215.
- [33] Klymenko, O. V.; Evans, R. G.; Hardacre, C.; Svir, I. B.; Compton, R. G. *J. Electroanal. Chem.* **2004**, *571*, 211–221.
- [34] Adams, R. N. *Electrochemistry at Solid Electrodes*; Marcel Dekker, New York, 1969.

Figures



(a) IDBA



(b) IDRA

Figure 1: Schematic diagram of the two interdigitated arrays investigated in this study.

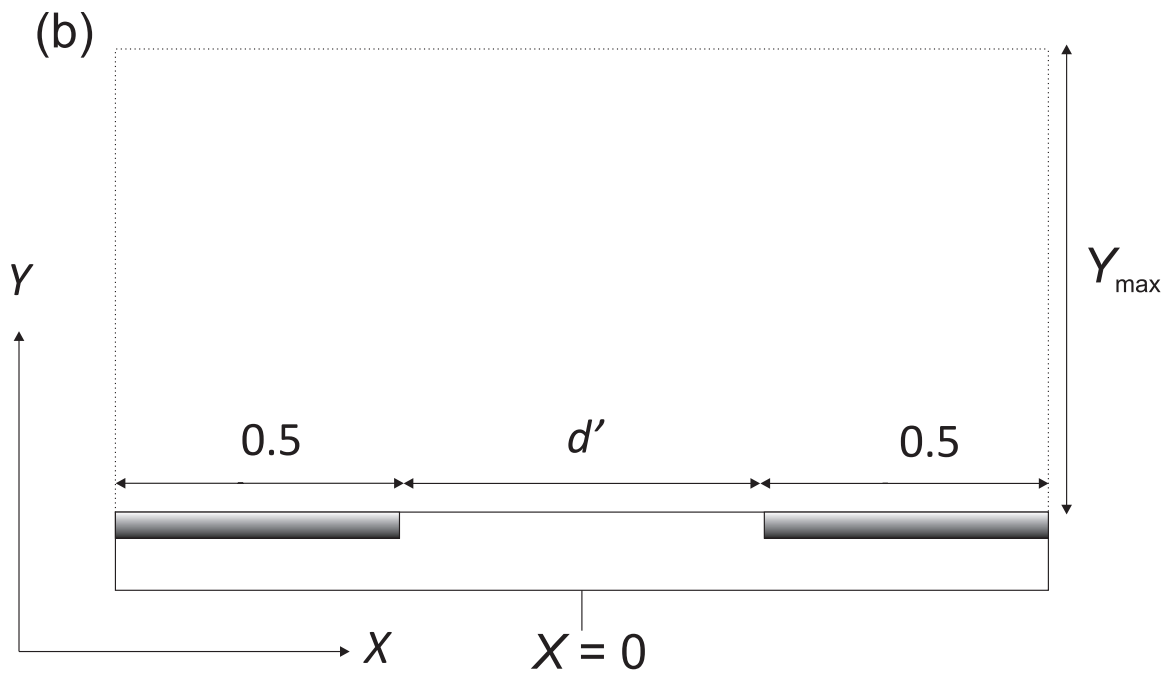
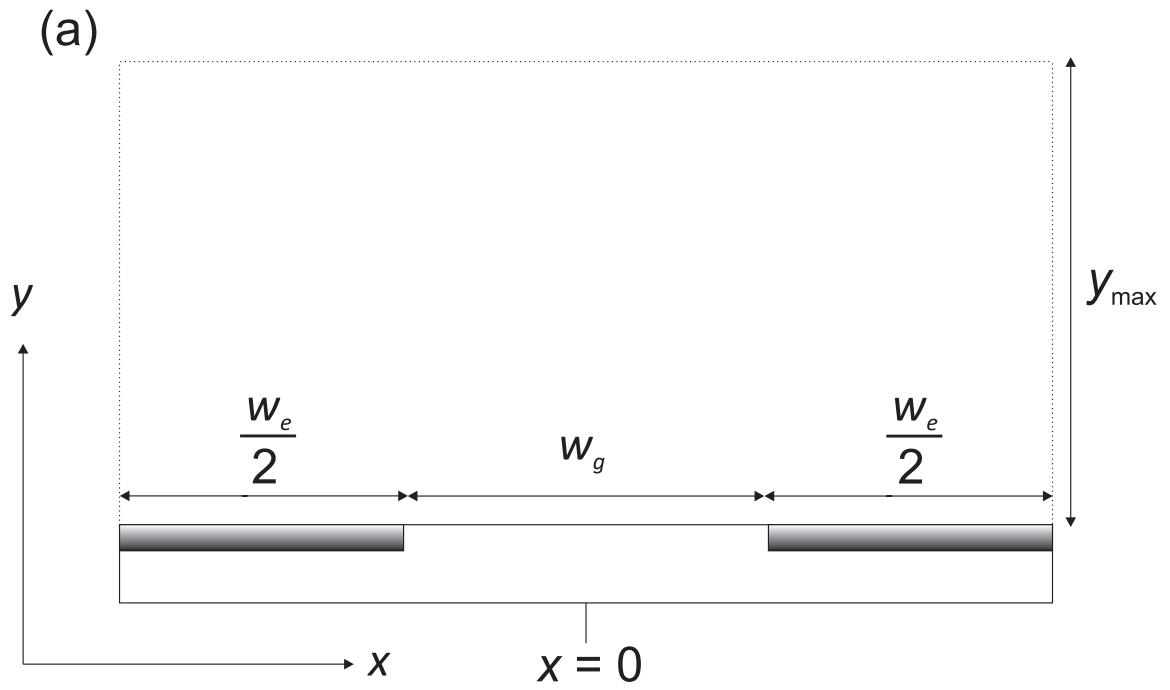


Figure 2: (a) Dimensional and (b) normalised simulation space used in the IDA model.

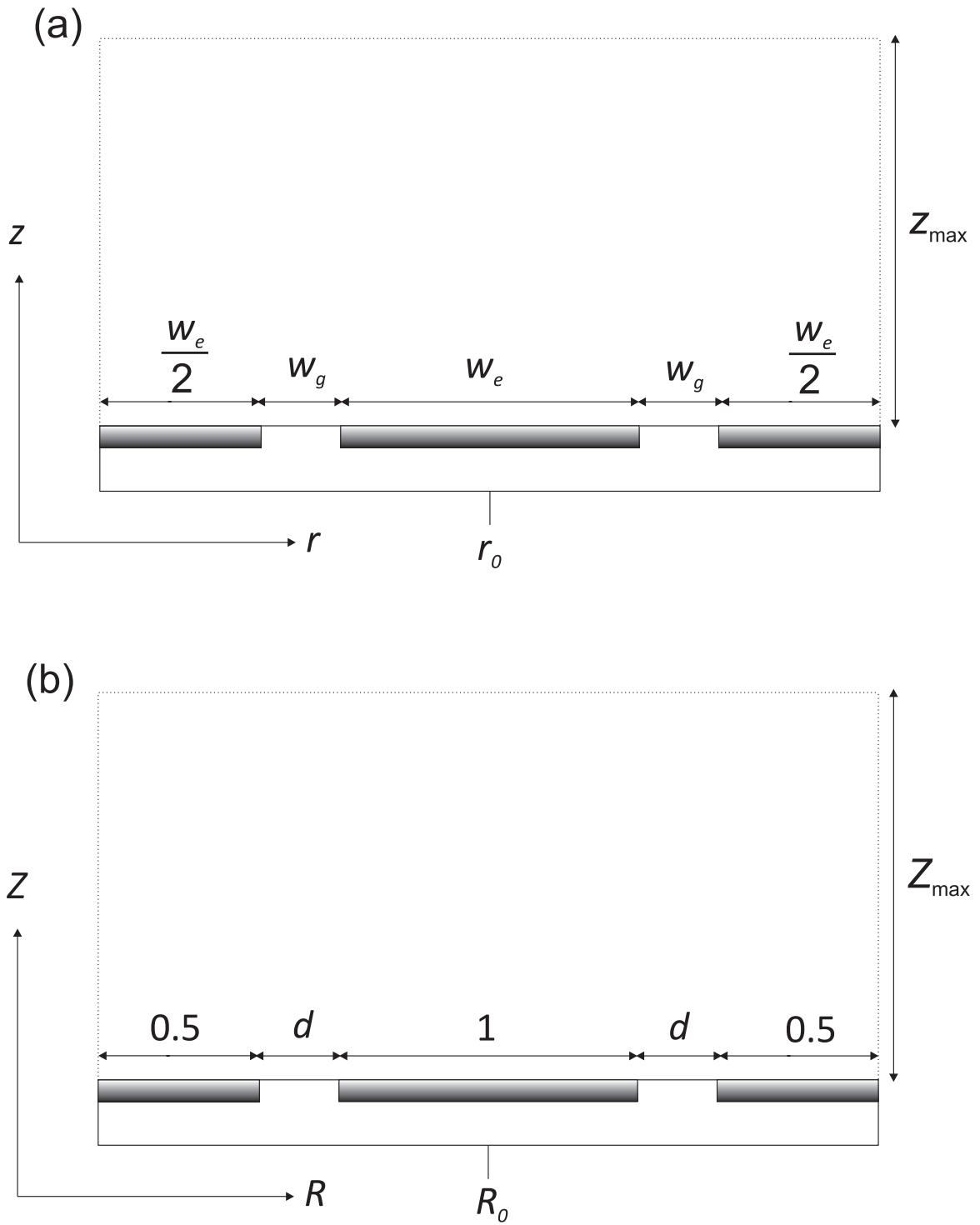


Figure 3: (a) Dimensional and (b) normalised simulation space used in the IDRA model.

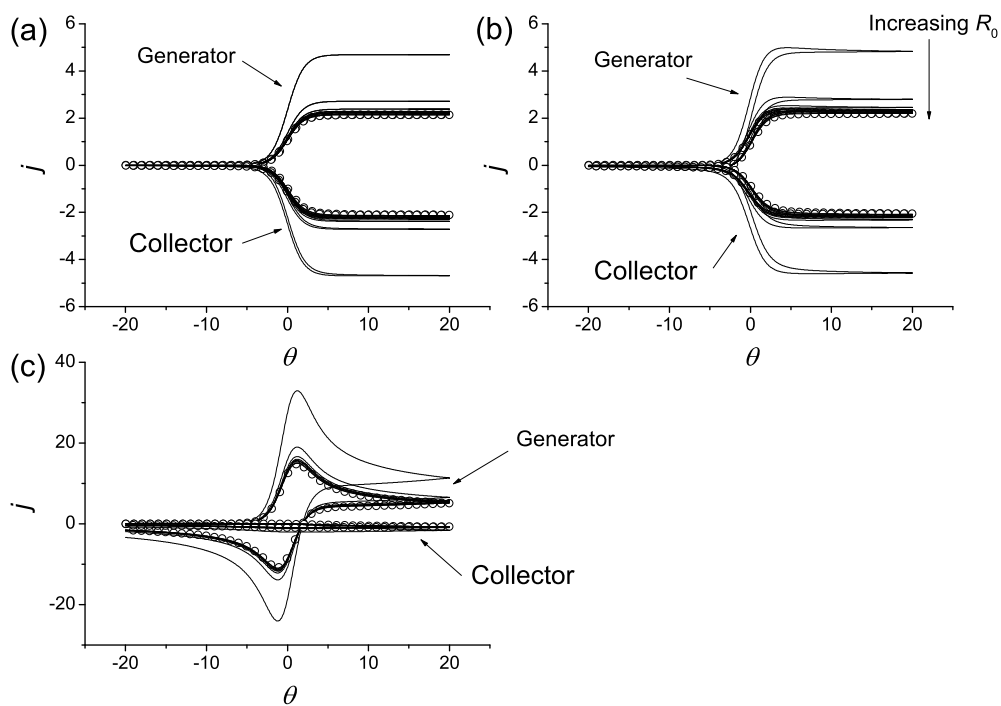


Figure 4: Simulated cyclic voltammograms for a one electron oxidation at a pair of electrodes in an IDBA (circles) and a pair in an IDRA at various values of R_0 ($= 2, 5, 10, 15, 20, 25, 50$ and 100 , lines). In all cases, $D'_B = 1$, $\alpha = 0.5$, $K^0 = 1000$. (a): $\sigma = 0.001$, (b): $\sigma = 1$ and (c): $\sigma = 1000$

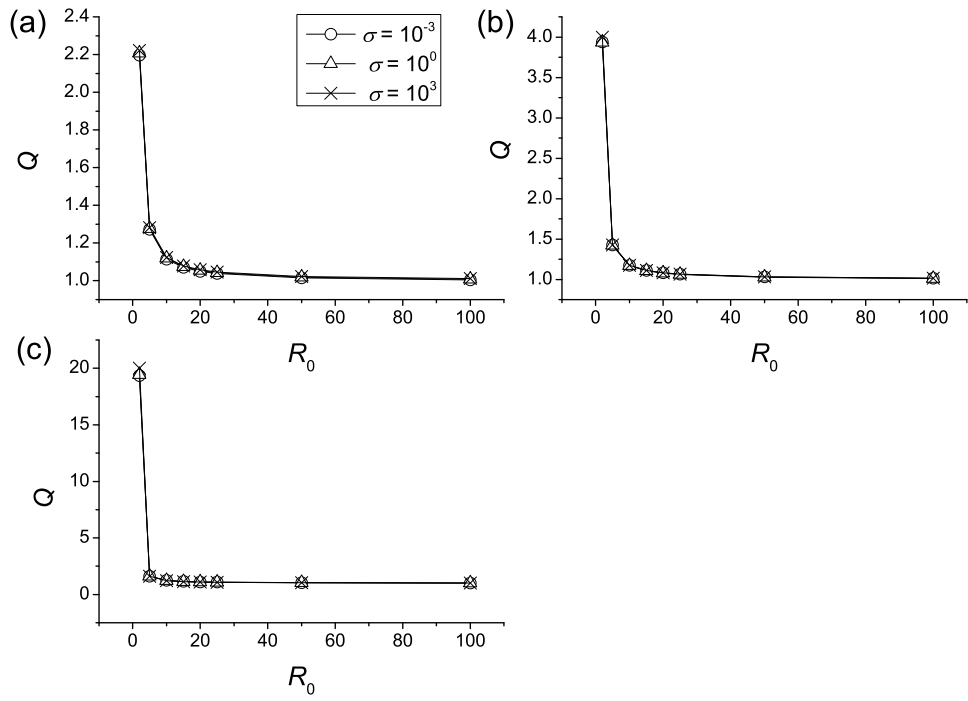


Figure 5: Values of Q for various R_0 for values of d' of (a): 0.1, (b): 0.5 and (c): 0.9. In each case, circles correspond to $\sigma = 0.001$, triangles to $\sigma = 1$ and crosses to $\sigma = 1000$. All other parameters as in Fig. 4.

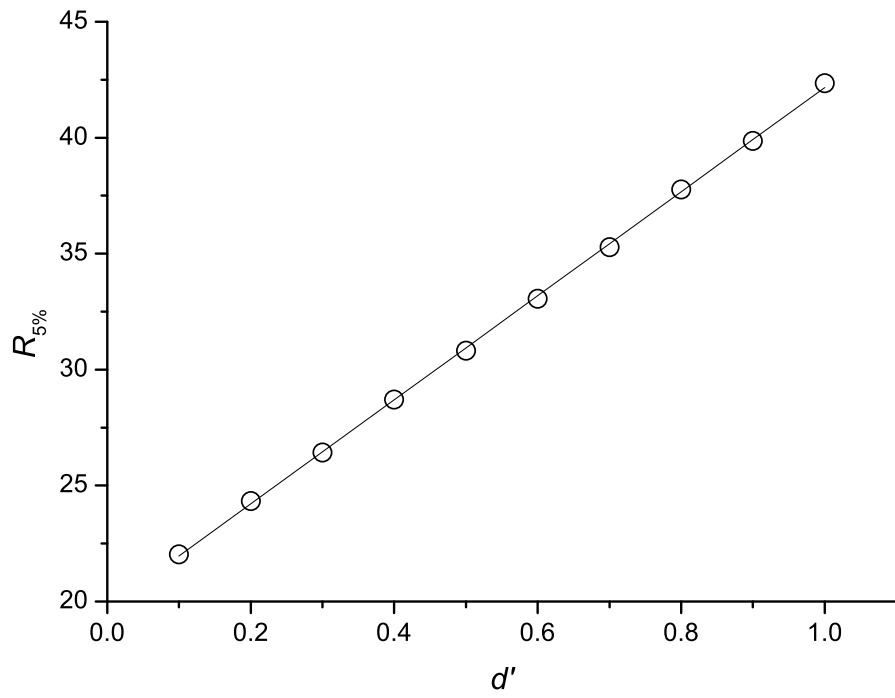


Figure 6: Values of $R_{5\%}$ (the value of R_0 necessary for an IDRA to produce a result within 5% of that for an IDBA) for various values of d' .

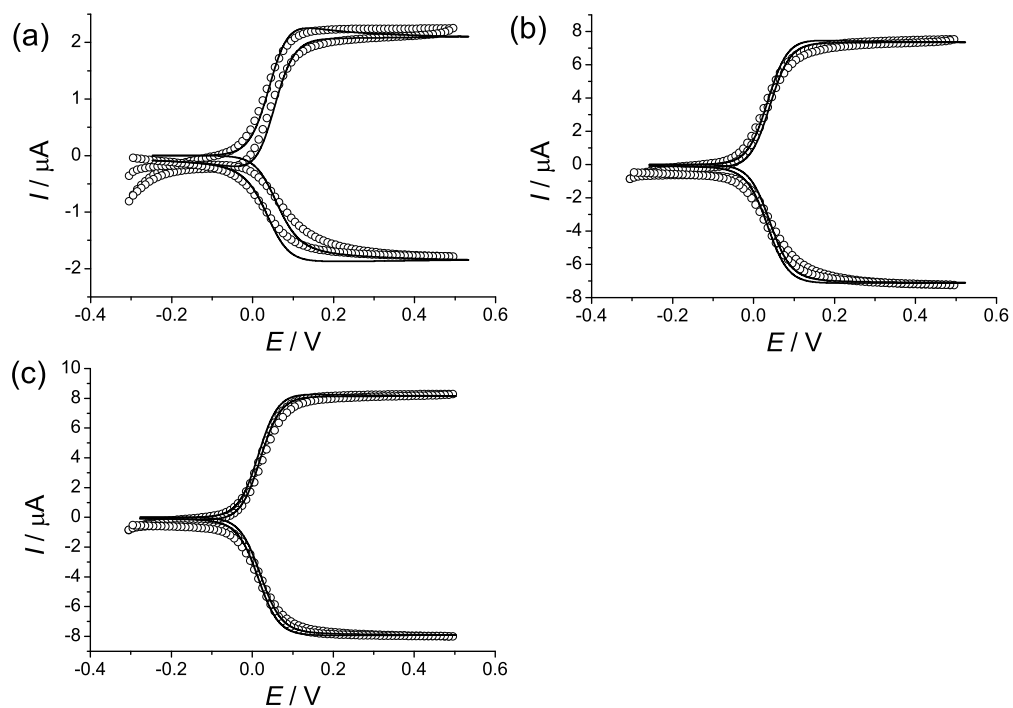


Figure 7: Experimental (circles) and simulated (lines) cyclic voltammograms of 1 mM potassium ferrocyanide at IDBA 1 (a), IDBA 2 (b) and IDBA 3 (c) electrodes (see Table 5). In all cases the scan rate was 50 mV s^{-1} .

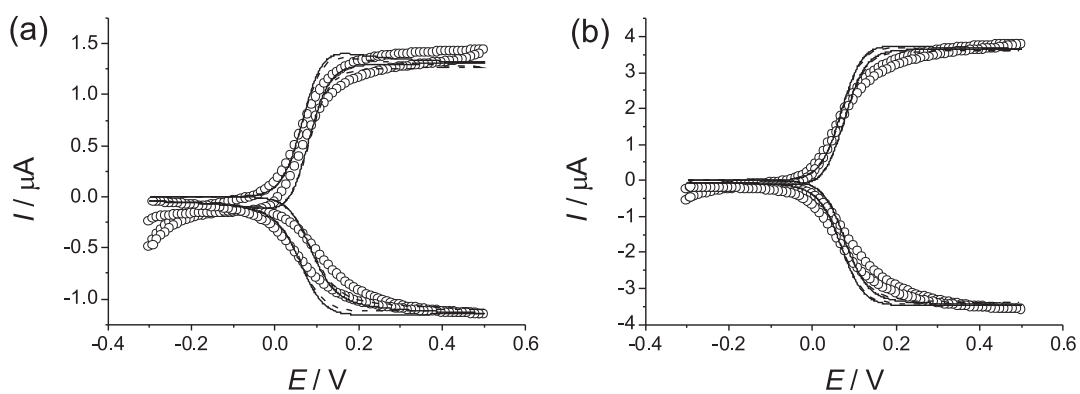


Figure 8: Cyclic voltammograms of 1 mM potassium ferrocyanide at IDRA 1 (a) and IDRA 2 (b) electrodes (see Table 5). In all cases the scan rate was 50 mV s^{-1} . Circles: Experimental data, solid lines: Simulations using the full IDRA model, dashed lines: Simulations approximating the rings as bands.

Tables

Parameter	Description	Units
α	Transfer coefficient	Unitless
c_i	Concentration of species i	mol m^{-3}
c_i^*	Bulk solution concentration of species i	mol m^{-3}
c_i^0	Concentration of species i at electrode surface	mol m^{-3}
D_i	Diffusion coefficient of species i	$\text{m}^2 \text{s}^{-1}$
E	Applied potential	V
E_f	Formal potential of A/B couple	V
F	Faraday constant = 96485	C mol^{-1}
I	Current	A
k^0	Electrochemical rate constant	m s^{-1}
l	Electrode length	m
ν	Scan rate	V s^{-2}
R	Gas constant = 8.314	$\text{J K}^{-1} \text{mol}^{-1}$
r	Radial coordinate in cylindrical space	m
r_0	Radius to centre of generator electrode in cylindrical simulation space	m
T	Temperature	K
t	time	s
w_e	width of electrode	m
w_g	width of inter electrode gap	m
x	x coordinate in Cartesian space	m
y	y coordinate in Cartesian space	m
z	z coordinate in cylindrical space	m

Table 1: List of symbols

Dimensionless Parameter	Definition
C_i	$\frac{c_i}{c_A^*}$
d'	$\frac{w_g}{w_e}$
D'_i	$\frac{D_i}{D_A}$
j (bands)	$\frac{I}{nFDc_A^*}$
j (rings)	$\frac{I}{2\pi nFr_0Dc_A^*}$
K^0	$\frac{w_e}{D_A}k^0$
Q	$\frac{I_{\text{ring}}^{\text{peak}}}{I_{\text{band}}^{\text{peak}}}$
R	$\frac{r}{w_e}$
σ	$\frac{Fw_e^2}{RTD_A}\nu$
θ	$\frac{RT}{F}E$
θ_f^\ominus	$\frac{RT}{F}E_f^\ominus$
τ	$\frac{D_A t}{w_e^2}$
X	$\frac{x}{w_e}$
Y	$\frac{y}{w_e}$
Z	$\frac{z}{w_e}$

Table 2: Normalised parameters. Species A refers to the species initially present in solution before the experiment/simulation begins.

τ	X	Y	Boundary condition(s)
$\tau < 0$	All X	All Y	$C_A = 1, C_B = 0$
$\tau \geq 0$	$-0.5 - \frac{1}{2}d < X \leq -\frac{1}{2}d$	$Y = 0$	$D'_A \left(\frac{\partial C_A}{\partial Y} \right) = K^0 C_A^0 \exp[-\alpha(\theta - \theta_f^e)] - K^0 C_B^0 \exp[(1 - \alpha)(\theta - \theta_f^e)]$ $D'_B \left(\frac{\partial C_B}{\partial Y} \right) = -D'_A \left(\frac{\partial C_A}{\partial Y} \right)$
	$\frac{1}{2}d \leq X < \frac{1}{2}d + 0.5$	$Y = 0$	$D'_A \left(\frac{\partial C_A}{\partial Y} \right) = -D'_B \left(\frac{\partial C_B}{\partial Y} \right)$ $C_B = 0$
	$X = -0.5 - \frac{1}{2}d$	All Y	$\frac{\partial C_i}{\partial X} = 0$
	$X = 0.5 + \frac{1}{2}d$	All Y	$\frac{\partial C_i}{\partial X} = 0$
	All X	$Y = Y_{\max}$	$\frac{\partial C_i}{\partial Y} = 0$

Table 3: Normalised boundary conditions for the IDBA model

τ	R	Z	Boundary condition(s)
$\tau < 0$	All R	All Z	$C_A = 1, C_B = 0$
$\tau \geq 0$	$R_0 - 0.5 < R \leq R_0 + 0.5$	$Z = 0$	$D'_A \left(\frac{\partial C_A}{\partial Z} \right) = K^0 C_A^0 \exp(-\alpha(\theta - \theta_f^\circ)) - K^0 C_B^0 \exp[(1 - \alpha)(\theta - \theta_f^\circ)]$ $D'_B \left(\frac{\partial C_B}{\partial Z} \right) = -D'_A \left(\frac{\partial C_A}{\partial Z} \right)$
	$R_0 - 0.5 - d \leq R \leq R_0 + 0.5 + d$	$Z = 0$	$D'_A \left(\frac{\partial C_A}{\partial Z} \right) = -D'_B \left(\frac{\partial C_B}{\partial Z} \right)$ $C_B = 0$
	$X = R_0 - 1 - d$	All Z	$\frac{\partial C_i}{\partial X} = 0$
	$X = 0.5 + 1 + d$	All Z	$\frac{\partial C_i}{\partial X} = 0$
	All R	$Z = Z_{\max}$	$\frac{\partial C_i}{\partial Z} = 0$

Table 4: Normalised boundary conditions for the IDRA model

Electrode	Bands/rings	Electrode width / μm	Gap width / μm	Number of pairs
IDBA 1	Bands	10	10	15
IDBA 2	Bands	5	2	42
IDBA 3	Bands	3	2	59
IDRA 1	Rings	10	10	12
IDRA 2	Rings	5	3	30

Table 5: Summary of geometries of electrode arrays used in this study. All the band electrodes are 2 mm in length.